Journal of Neural Engineering

ACCEPTED MANUSCRIPT

Decoding hindlimb kinematics from descending and ascending neural signals during cat locomotion

To cite this article before publication: Yaser Fathi *et al* 2021 *J. Neural Eng.* in press https://doi.org/10.1088/1741-2552/abd82a

Manuscript version: Accepted Manuscript

Accepted Manuscript is "the version of the article accepted for publication including all changes made as a result of the peer review process, and which may also include the addition to the article by IOP Publishing of a header, an article ID, a cover sheet and/or an 'Accepted Manuscript' watermark, but excluding any other editing, typesetting or other changes made by IOP Publishing and/or its licensors"

This Accepted Manuscript is **© 2020 IOP Publishing Ltd**.

During the embargo period (the 12 month period from the publication of the Version of Record of this article), the Accepted Manuscript is fully protected by copyright and cannot be reused or reposted elsewhere.
As the Version of Record of this article is going to be / has been published on a subscription basis, this Accepted Manuscript is available for reuse under a CC BY-NC-ND 3.0 licence after the 12 month embargo period.

After the embargo period, everyone is permitted to use copy and redistribute this article for non-commercial purposes only, provided that they adhere to all the terms of the licence https://creativecommons.org/licences/by-nc-nd/3.0

Although reasonable endeavours have been taken to obtain all necessary permissions from third parties to include their copyrighted content within this article, their full citation and copyright line may not be present in this Accepted Manuscript version. Before using any content from this article, please refer to the Version of Record on IOPscience once published for full citation and copyright details, as permissions will likely be required. All third party content is fully copyright protected, unless specifically stated otherwise in the figure caption in the Version of Record.

View the article online for updates and enhancements.

This content was downloaded from IP address 139.82.115.33 on 14/01/2021 at 16:34

Decoding hindlimb kinematics from descending and ascending neural signals during cat locomotion

Yaser Fathi and Abbas Erfanian*

Department of Biomedical Engineering, School of Electrical Engineering, Iran University of Science and Technology (IUST), Iran Neural Technology Research Centre, Tehran, Iran

*E-mail: erfanian@iust.ac.ir

Abstract

Objective. The main objective of this research is to record both sensory and motor information from the ascending and descending tracts within the spinal cord for decoding the hindlimb kinematics during walking on the treadmill. *Approach*. Two different experimental paradigms (i.e., active and passive) were used in the current study. During active experiments, five cats were trained to walk bipedally while their hands kept on the front frame of the treadmill for balance or to walk quadrupedally. During passive experiments, the limb was passively moved by the experimenter. Local field potential (LFP) activity was recorded using a microwire array implanted in the dorsal column (DC) and lateral column (LC) of the L3-L4 spinal segments. The amplitude and frequency components of the LFP formed the feature set, and the elastic net regularization was used to decode the hindlimb joint angles. *Main results.* The results show that there is no significant difference between the information content of the signals recorded from the DC and LC regions during walking on the treadmill, but the information content of the DC is significantly higher than that of the LC during passively applied movement of the hindlimb in the anesthetized cats. Moreover, the decoding performance obtained using the recorded signals from the DC is comparable with that from the LC during locomotion. But, the decoding performance obtained using the recording channels in the DC is significantly better than that obtained using the signals recorded from the LC. The long-term analysis shows that robust decoding performance can be achieved over 2-3 months without a significant decrease in performance. *Significance*. This work presents a promising approach to developing a natural and robust motor neuroprosthesis device using descending neural signals to execute the movement and ascending neural signals as the feedback information to control the movement.

Keywords: Neural decoding, hindlimb kinematics, ascending tracts, descending tracts, spinal cord, dorsal column, lateral column.

Accepted Manuscript

1. Introduction

Functional electrical stimulation (FES) is a promising technique to restore the lost limb function in people with paralyzed extremities. FES produces muscle contraction through electrical stimulation of the nervous system. Providing robust and natural command signals is a pivotal issue to develop such a system in clinical platforms [1]. Neural recordings can be utilized to decode the intended action and translated into a command signal for a neuroprosthetic device. In addition to the command signal, sensory information can be recorded to estimate the limb state in a closed-loop manner for adapting the controller to environmental changes and improving the control performance in response to perturbations [1].

During the last decade, decoding the hindlimb kinematics and muscle EMGs from cortical neuronal activity during bipedal walking of monkey [2] and rat [3] and during quadrupedal locomotion in rats [4, 5] have been investigated. In [4], it has been tested if multiple movement-related variables can be decoded by using the simultaneous activity of populations of cells in the hindlimb/trunk area of the rat motor cortex during quadrupedal locomotion in rats.

Recordings from peripheral nerve have also been used to decode the kinematic information [6-8], to detect gait event [9], to recover motor activation [10] using cuff electrodes, and to extract the grasp information (e.g., grip types and single finger movement) using intra-fascicular electrodes [11, 12]. The cuff recordings provide information from different afferent and efferent signals, which limit the resolution of nerve cuffs. The cuff recordings may be also contaminated with EMG interference from nearby muscles. Moreover, multiple nerve cuff electrode recordings are required to acquire the information from the entire limb during a complex movement such as locomotion [1, 13-15].

Dorsal root ganglia (DRG) has been also considered as an alternate source for recording sensory information. The dorsal root ganglia contain cell bodies of sensory neurons that carry sensory information from the periphery to the spinal cord. Studies with microelectrode array implanted chronically in the DRG of cats have shown that neural activity recorded simultaneously from several DRG neurons can be used to estimate the kinematics (i.e., position, velocity, and acceleration) of the hip, knee, and ankle joints during locomotion [16-18] and during passive movement of the hindlimb [19-23]. Recently, it has been demonstrated that recordings from the surface of the dorsal root ganglion can be modulated by the passive movement of the hindlimb [24].

Accepted Manuscript

The recordings from the ventral spinal roots can also be a potential source for extracting motor control signals from the nervous system. The ventral spinal roots contain the axons of motor neurons in the ventral horn of the spinal cord, which innervates the skeletal muscle. In [25, 26], it was demonstrated that it is possible to record from motor axons in the ventral root. In [26], it was also shown that the recordings from the ventral roots could be used to estimate the gait phases. However, they reported that accurate targeting of the ventral root was difficult through their experiments. Moreover, although the ventral root can be a potential source for the extraction of motor commands in people with amputees, in the case of spinal cord injury, the ventral root cannot provide the intention information for a movement.

Spinal cord recordings have been also proposed as an alternative source of information for decoding limb kinematics. The modulation of dorsal spinocerebellar neurons responses to the limb movement has been investigated [27-30]. The spinocerebellar system is one of the main central projections of the muscle receptors. It was reported that the activities of dorsal spinocerebellar neurons encode the global parameters of limb movement and posture rather than the specific muscle or joint parameters. The dorsal horn is an alternate location for extracting sensory information. The central branch of the sensory axon enters the dorsal horn of the spinal cord [31]. The dorsal horn recordings in rats have been already used for detecting the sensory events generated by electrical stimulation [32] or to decode the bladder pressure [33, 34]. In previous work, we introduced decoding the hindlimb kinematics using neural recordings from the dorsal horn cells during passive hindlimb movements of anesthetized cats [35, 36].

A possible source of extracting kinematics information within the spinal cord is the descending pathways. The descending pathways, including corticospinal tracts and rubrospinal tracts, have a significant role in controlling balance, posture, locomotion, and reaching [37-40]. It was shown that there is a correlation between the neural signals recorded from the descending tracts and the forelimb movements [41-44]. Recently, they demonstrated that the EMG signals of the forelimb flexor and extensor can be decoded from the corticospinal tract signals [45, 46].

In this study, for the first time, we will show that the neural signals recorded from the descending tracts of the spinal cord (i.e., lateral column) can be used to decode the hindlimb kinematics during walking on the treadmill. Moreover, the feasibility of decoding the hindlimb kinematics from the dorsal column is evaluated. The dorsal column which contains ascending sensory pathways, carry information about tactile sensations and proprioception to the brain stem [31].

Accepted Manuscript

An important issue in the design of FES for restoring motor function is the feedback information that needs to be stable over a long period. In this paper, we address the stability of spinal cord recording by evaluating the decoding performance over long-term. Another critical issue in decoding kinematic information from neural signals is the decoding model. In this paper, we employ a robust parsimonious linear decoding method known as elastic net [47, 48] to decode limb joint angles using extracted local field potential (LFP) features.

2. Materials and methods

The experiments were conducted on five male cats (3.1-4.2 kg). All surgical procedures and experimental protocols involving animal models described in this paper were approved by the Institutional Animal Care and Ethics Committee of Iran Neural Technology Research Center, Iran University of Science and Technology. The whole protocols and methods were performed in accordance with the recommendations and relevant guidelines for the care and use of laboratory animals.

2.1. Microwire array fabrication

The recordings were made from the spinal cord using a custom-made microelectrode array. The electrode array was made from Teflon-insulated tungsten wires with diameters of 50 μm (No. 79550, A-M Systems, USA) and an inter-electrode spacing of 600-800 μm. To record from both sensory and motor spinal tracts, the array was designed to cover the dorsal column (DC) region as well as the lateral column (LC).

The dorsal and lateral columns, at the L3-L4 spinal segments, typically cover a span of ~0.0-1.5 mm and ~1.5-3.0 mm laterally from the midline to the left side and a span of ~0.0-1.5 and ~1.5-2.5 mm in depth from the dorsal surface. The recording electrode lengths varied from 0.5 to 2.5 mm, which allowed them to fully penetrate the dorsal and lateral columns. At least two electrode arrays of varying sizes were prepared to enable the surgeon to some flexibility in the placement of the array. In 2×4 arrays, the second row was designed in a similar way but to target different depths compared to the first row to increase the chance of placing the electrodes in the desired area (figure 1(a)). Teflon insulated microwires were soldered to the header strip connector through multi-strand flexible wires.

Accepted Manuscript

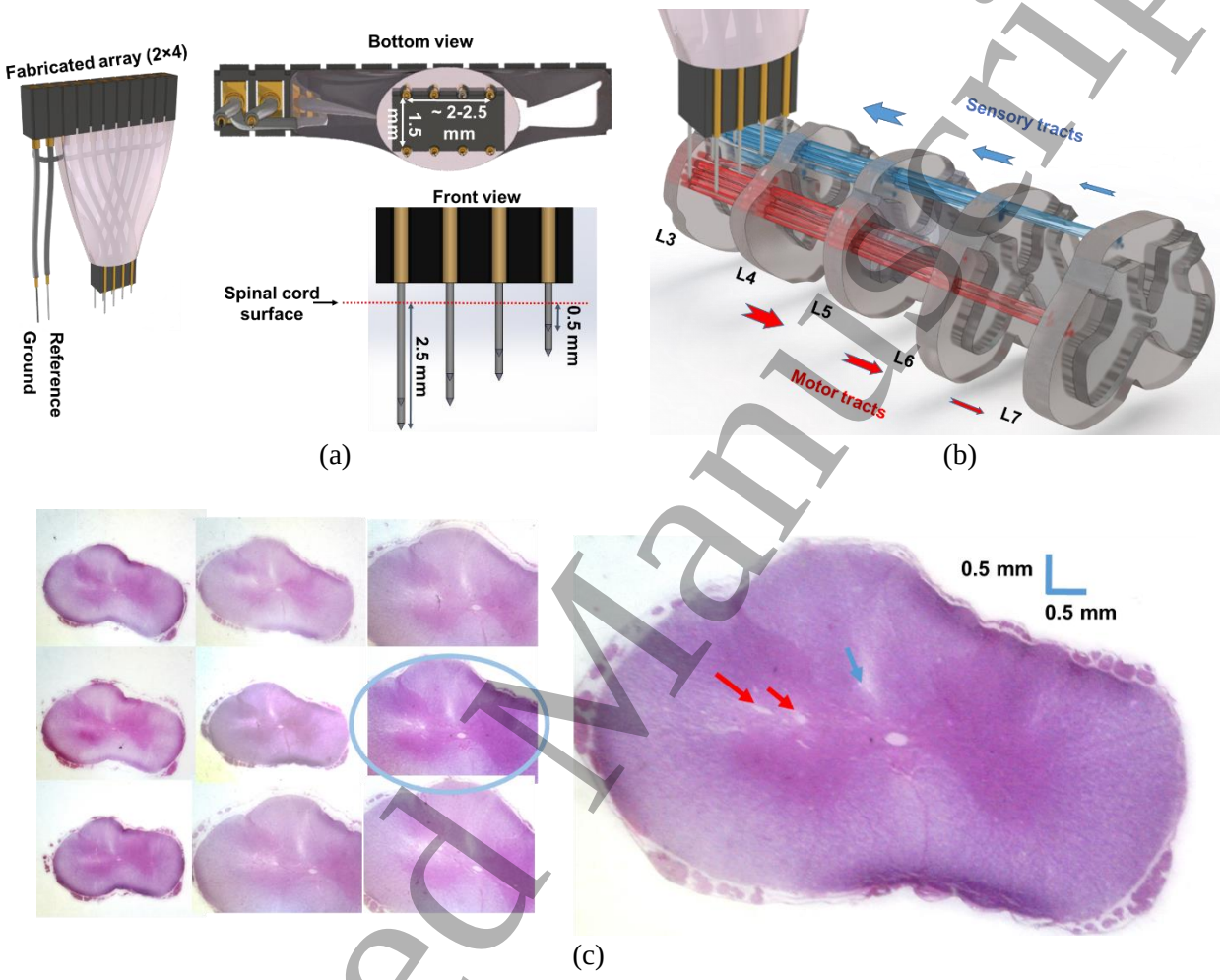

Figure 1. Electrode fabrication and implantation overview. (a) Schematic of the custom-made microwire array with connector, reference, and ground wires. (b) Schematic figure showing ascending and descending tracts in the spinal cord and how and where the microwire array was implanted. (c) A typical histological analysis showing different slices of the segment that the microwires were implanted.

2.2. Surgical procedure and implantation process

2.2.1. Implantation process. Initial anesthesia was induced with an intramuscular injection of ketamine (20 mg/kg) into the cranial thigh muscle. Then, the animals were maintained at a surgical level of anesthesia under isoflurane inhalation (1.0%–3.0% in O2). A partial 4×4 mm laminectomy was performed over the left (with respect to the rostral-caudal vector) L4 vertebra. Four screws were inserted into the bone of L4 vertebra in the more bulky regions. We utilized these screws as an anchor for the array and connector. The array and connector will later be fixed to the vertebra

Accepted Manuscript

by using dental acrylic. After laminectomy and drilling screws to the vertebra, a 28-gauge sterile needle bent at 90 degrees was employed to make an incision in the dura matter. Then, a 4×4mm section of dura matter below the left L4 vertebra was gently resected using a microscissor to expose the spinal cord. The animal was then mounted in a stereotactic frame (SN-1N, Narishige Group Product, Japan) and the spinal L5 vertebra was clamped tightly to the frame to restrict the spinal cord movement and stabilize it during array insertion. The microelectrode connector was then attached to a micromanipulator (SM-15, Narishige Group Product, Japan) that could control the three-dimensional positioning of the electrode with a minimum graduation of 10 μm. The electrode array was then positioned at the locations within the L3-L4 segments to cover the dorsal and lateral columns (figure 1(b)). The recording ground wire was attached to a bone screw inserted in the L3 or L5 vertebra and the reference wire was placed proximally in the epidural space. A layer of sylgard 184 covered the surface of the spinal cord. After that, the dental acrylic was applied to fix the implantation array to the bone.

2.2.2. *Post-surgical treatment and care*. After surgery, the animals were transferred to a recovery room separated from other animals. While regaining consciousness, the possible excessive struggle of the animal may damage the implant or spinal cord. Hence, low-dose meloxicam (0.2 mg/kg) was subcutaneously administered before transferring the animal to the recovery room. Cefazolin (30mg/kg) was intramuscularly injected twice daily for a week after surgery. Moreover, tramadol (2mg/kg) was intramuscularly injected daily for relieving pain for two or three days after surgery. In a few days after surgery, cats may lose food appetite and need more attention. Excretion and urination of cats were also monitored every day to check possible abnormalities in the urinary system. During the first week after implantation, abnormal gate or posture might appear. These abnormalities may be due to the electrode placement in the spinal cord tissue or movement restriction of vertebrae and usually will be eliminated after one to three weeks by encouraging the cat to walk gradually.

2.2.3. Histology. For the histology, the animal was deeply anesthetized and a low-level direct current (15 μA for 15 s) was delivered through the electrodes to make electrolytic lesions at the recording sites. The microelectrode array was then removed and the spinal cord was harvested and submerged in a fixative solution (formaldehyde 10%). The spinal cord was kept in the fixative solution for a few days to permit the tissue to set and become sufficiently firm to slice. Then, the

Accepted Manuscript

tissue was processed and embedded in a paraffin block, sliced at 5 μm using a vibratome, placed onto slides, and stained with Hematoxylin and Eosin (H&E). Further microscopic examination was performed and the cavities produced at the tip of the electrodes were checked by a pathologist. Figure 1(c) shows a typical histological analysis to test the implantation process of this experiment. This analysis shows that the dimensions of the designed electrode array are suitable for electrode placement in the desired area.

2.3. Experimental procedure

All cats were trained before surgery to walk freely on a moving treadmill at the speed of about 0.14-0.2 m/s. Two different experimental paradigms, active and passive experiments, were considered in this study. Active experiments were performed during full consciousness, while passive experiments were conducted during anesthesia. During active experiments, cats freely walked on the treadmill. Three cats (1, 4, and 5) were trained to walk bipedally while keeping their hands on the front frame of the treadmill for balance. Two other cats (cats 2 and 3) walked quadrupedally while four hands and legs were on the treadmill during walking (see figure 2 and supplementary video). Animals were encouraged to walk by rewarding pellet food. During passive experiments, cats were mounted in a modified stereotaxic that allowed the hindlimb to hang freely in space. The left hindlimb was manually moved by the experimenter to simulate a locomotion pattern (see supplementary video).

The recordings were performed almost once a week during normal walking on the treadmill and every month during passive movement. During each day of the active experiment, 1-3 sessions, and on each day of the passive experiment, five recording sessions were performed. The resulting dataset is summarized in table 1. The durability of long-term recording for each cat was different. The decoding performance began to decrease after 87 days for cat 1, after 97 days for cat 2, after 61 days for cat 3, after 74 days for cat 4, and after 71 days for cat 5. Hence, different sessions of experiments were performed for each cat (table 1). The duration of each recording session was between 2-4 min.

2.4. Joint angle measurements

The hindlimb kinematics were captured by the high-speed (1-megapixel resolution) motion capture system (Vicon Motion Systems Ltd., UK) at 50 fps with three cameras perpendicular to the sagittal plane on the left at a distance of approximately 2 m from the animal. The reflective markers were

Accepted Manuscript

attached to the iliac crest, greater trochanter (hip joint), lateral condyle of the femur (knee joint), lateral malleolus (ankle joint), and the distal end of the fifth metatarsophalangeal (MTP) joint of the cats. Motion capture software (Tracker 2.2, Vicon, UK) was used to acquire the coordinate of the markers. Using five marker positions, three joint angles (ankle, knee, and hip) were calculated using a custom Matlab program. Motion data were then down-sampled to 10 Hz.

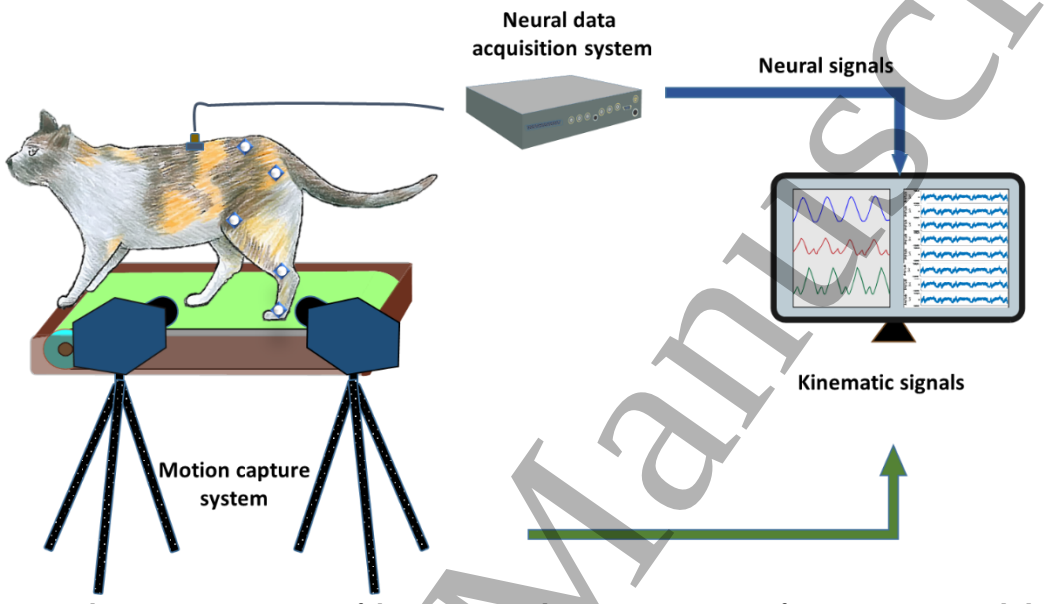

Figure 2. Schematic representation of the experimental setup. Kinematics information was recorded using a motion capture system. Neural signals were recorded during walking on a treadmill and converted from analog to digital using a data acquisition system and were then used to decode the joint angles in a desktop computer.

Table 1. Summary of data collected from each cat.

Cat	Walking style	Recording durability (days)	Implanted array dimension	Number of sessions (active/passive)	Duration of each recording (min)
1	Bipedal	87	1 × 4	26 (16/10)	4
2	Quadrupedal	97	1 × 4	30 (15/15)	4
3	Quadrupedal	61	2 × 4	19 (14/5)	3
4	Bipedal	74	2 × 4	24 (14/10)	3
5	Bipedal	71	2 × 4	24 (14/10)	2

2.5. Neural signal recording and preprocessing

Neural signals were recorded during walking on a treadmill and passive movement using a data acquisition system (USB-ME64 system, Multichannel Systems Reutlingen, Germany) at 20 kHz sampling rate. The recorded raw signals were down-sampled to 1 kHz and band-pass filtered

Accepted Manuscript

between 0.5 and 300 Hz using an elliptic filter of order two to extract LFP signal. Then, the signals were digitally notch filtered at 50, 100, and 150 Hz to remove power line interference.

The average amplitude of the LFP signal (ALFP) and the average of the power spectrum in the three logarithmically spaced frequency bands (0.5-30 Hz, 30-120 Hz, and 120-300 Hz) were used as the features to decode the kinematic information. In this work, we refer to these three bands as the low-frequency (LF), mid-frequency (MF), and high-frequency (HF) bands. To extract the features, the short-time Fourier transform (STFT) was applied to the LFP signal to generate power spectra over time with a 500 ms Hanning window with 80% overlap. The same window was used to calculate the ALFP feature. Ten time-lags of each feature ($t, t-100\ ms, \dots, t-900\ ms$) were also included in the feature set at time *t* (we will show later that the time-lags of each feature has a contribution to the decoding process). Hence, for each recording channel, we extracted 40 (4×10) features, which totally resulted in 160 and 320 features for 1×4 and 2×4 arrays, respectively (figure 3).

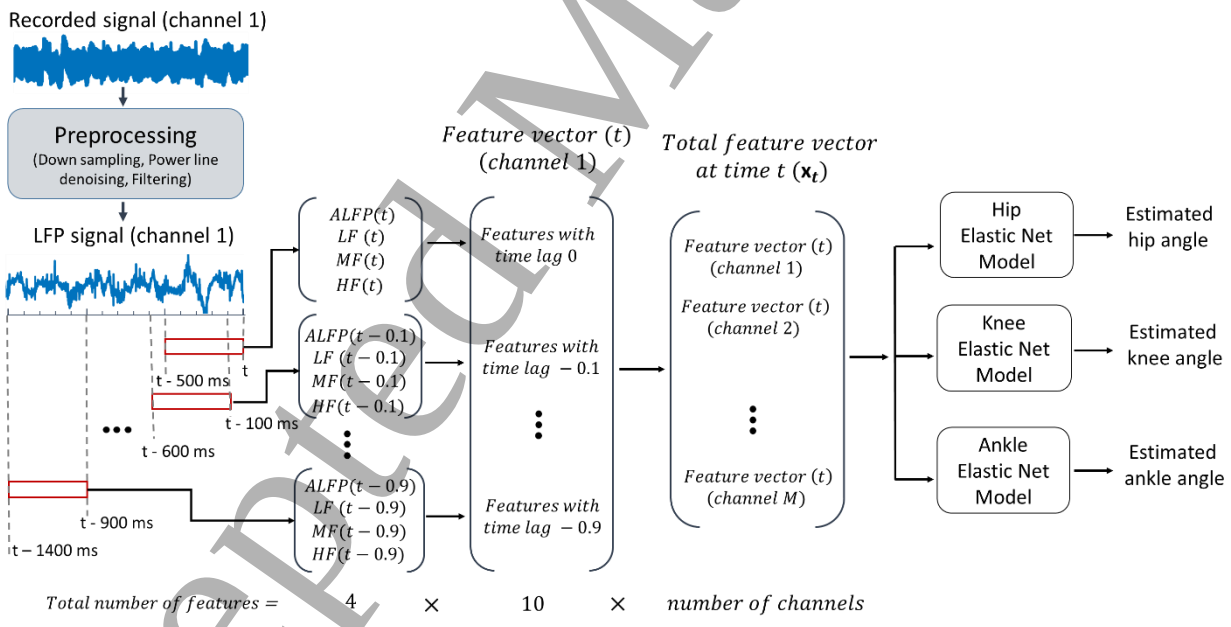

Figure 3. Schematic illustration of the neural signal processing and feature extraction. The features were extracted from 500-ms windows with 80% overlap and applied to each decoding model for estimating the joint angle. A specific decoding model was designed for each joint angle.

2.6. Decoding model

Decoding neural signals to predict the limb kinematics can be considered as a regression problem. Regression analysis is a statistical technique for determining the relationship between a response

Accepted Manuscript

variable (e.g., *y*) and one or more independent (predictors) variables (e.g., **x)**. To be specific, consider a general regression model defined by

$$y_t = f(\mathbf{x}_t) + \varepsilon_t \quad (1)$$

where y_t is the joint angle (hip, knee, or ankle angle), $\mathbf{x}_t$ is the feature vector at time *t* (i.e., ALFP, LF, MF, and HF extracted from all channels and their ten time-lags as depicted in figure 3), and ε is an additive white-noise term of zero mean and variance σ^2. Linear regression approximates $f(.)$ by a linear model as

$$\hat{y}_t = \mathbf{x}_t^{\mathrm{T}}\boldsymbol{\beta} + \beta_0 \quad (2)$$

For each joint angle, a model is identified (figure 3). The size of the coefficient vector $\boldsymbol{\beta}$ is equal to the size of the feature vector $\mathbf{x}_t$ and each element of the coefficient vector $\boldsymbol{\beta}$ corresponds to one feature element in the feature vector $\mathbf{x}_t$. We define each element of the vector $\boldsymbol{\beta}$ as $\beta_{feature,lag,ch}$, where *feature* can be one of ALFP, LF, MF, or HF, *lag* specifies the time-lag of the feature, and *ch* specifies the channel. A conventional method to estimate the coefficient vector ($\boldsymbol{\beta}$ and β_0) is the ordinary least squares (OLS). The OLS estimates are obtained by minimizing the residual sum of squares. To improve the performance of the OLS algorithm, different penalization techniques have been proposed [47, 48]. In this paper, we used the *elastic net regularization*. Similar to the lasso, the elastic net simultaneously does automatic variable selection and continuous shrinkage, and it can select groups of correlated variables. The elastic net criterion is defined as follows [47, 48]:

$$L(\alpha, \boldsymbol{\beta}) = |\mathbf{y} - \mathbf{X}\boldsymbol{\beta}|^2 + \lambda P_\alpha(\boldsymbol{\beta}) \quad (3)$$

where $\mathbf{y} = [y_1, y_2, \dots, y_N]^T$ and $\mathbf{X} = [\mathbf{x_1}, \mathbf{x_2}, \dots, \mathbf{x_N}]^T$ are *N* observation pairs and P_α is the penalty term of the elastic net, which is a convex combination of the lasso and ridge penalty terms as follows:

$$P_\alpha(\boldsymbol{\beta}) = \alpha\|\boldsymbol{\beta}\|_{l_2}^2 + (1-\alpha)\|\boldsymbol{\beta}\|_{l_1} \quad (4)$$

when $\alpha = 0$ or $\alpha = 1$ elastic net is similar to lasso or ridge, respectively. Any values of α between 0, 1 make a compromise between these two methods. The coefficient vector $\boldsymbol{\beta}$ is estimated using the least angle regression (LARS) algorithm for the elastic net (LARS-EN), which is a simple modification of a stepwise algorithm [49]. Briefly, LARS starts with all coefficients set to zero. Then it searches the predictor with the largest absolute correlation with the response and takes the step in the direction of this predictor up to the point that another predictor becomes as much

Accepted Manuscript

correlated with the current residual. At this stage, LARS proceed in a new direction equiangular between the two predictors until another predictor enters the subset, and so on.

Input variables are in standardized form by first removing the mean and then dividing by the standard deviation. Mean and standard deviation for each dimension of input is calculated and updated when each new observation is received:

$$x_{t,j} = (x^*_{t,j} - m_{t,j})/s_{t,j} \tag{5}$$

where $x^*_{t,j}$ is the observed signal at time *t* and

$$m_{t,j} = \frac{1}{t}\sum_{n=1}^{t} x^*_{n,j}$$

$$s_{t,j} = (\frac{1}{t}\sum_{n=1}^{t}(x^*_{n,j} - m_{t,j})^2)^{\frac{1}{2}}$$

2.7. Data analysis

2.7.1 Performance evaluation

To assess the performance of the decoding the limb kinematics, the normalized root-mean-square (NRMS) of the estimation error and the coefficient of determination, R^2 value were used. The NRMS and R^2 were defined as

$$\text{NRMS} = \frac{\sqrt{\frac{1}{N}\sum_{n=1}^{N}(y_n - \hat{y}_n)^2}}{max(\mathbf{y}) - min(\mathbf{y})} \tag{6}$$

$$R^2 = 1 - \frac{\sum_{n=1}^{N}(y_n - \hat{y}_n)^2}{\sum_{n=1}^{N}(y_n - \bar{y})^2} \tag{7}$$

where y is the measured joint angle and $\bar{y}$ is its mean value, $\hat{y}$ is the estimated angle, and *N* is the number of data points. Moreover, in order to evaluate the information content of the neural signals, the mutual information (MI) was calculated between LFP features and the hindlimb kinematics. In contrast to the linear correlation coefficient, which measures the linear relationship between variables, MI takes into account both linear and nonlinear dependency. In this work, mutual information was estimated using adaptive partitioning algorithm proposed in [50]. We used three-fold cross-validation for training and testing the model. During each fold, the coefficient vector β and the parameter λ were estimated and validated using five-fold cross-validation on the training data. The number of fold was selected by trial and error to obtain better performance. The recorded data were split into blocks of contiguous samples of recorded data. Training, validation, and test were performed on each data file obtained during each session of the experiment. In each round of

Accepted Manuscript

three-fold, 67% of data was assigned for training and model parameter selection, and the remaining 33% of data were assigned to test the model. Finally, the average of the decoding performance across three folds and all sessions of the experiment was computed.

2.7.2 Regression analysis

Based on the coefficients of the decoding models (2), three quantities were defined to estimate the contributions of each recording channel, time lag, and feature type (LF, MF, HF, and ALFP) in the decoding model of each joint angle as follows [51, 52]:

$$W_s(ch) = \frac{\sum_{feature}\sum_{lag}|\beta_{feature,lag,ch}|}{\sum_{feature}\sum_{lag}\sum_{ch}|\beta_{feature,lag,ch}|} \quad (8)$$

$$W_f(feature) = \frac{\sum_{ch}\sum_{lag}|\beta_{feature,lag,ch}|}{\sum_{feature}\sum_{lag}\sum_{ch}|\beta_{feature,lag,ch}|} \quad (9)$$

$$W_t(lag) = \frac{\sum_{feature}\sum_{ch}|\beta_{feature,lag,ch}|}{\sum_{feature}\sum_{lag}\sum_{ch}|\beta_{feature,lag,ch}|} \quad (10)$$

where $W_s(ch)$, $W_f(feature)$, and $W_t(lag)$ are representing the importance of each recording electrode, each feature, and each time lag in decoding performance, respectively. $\beta_{feature,lag,ch}$ represents the coefficient of the regression model for a feature at a specific time-lag extracted from a channel. $W_s(ch)$ for each recording electrode is calculated by summing up the absolute values of decoding coefficients of that electrode across time lags and features and then normalized by the absolute sum of all coefficients. $W_f(feature)$ and $W_t(lag)$ were also calculated in the same way based on (9) and (10), respectively.

2.7.3 Statistical analysis

All data analyses and decoding models were performed with customized algorithms written in MATLAB. One-way and two-way analyses of variance (ANOVA) followed by the Tukey's HSD posthoc test were used to assess the statistical significance of the results and differences and a confidence level of 95% ($p < 0.05$) was chosen to indicate a significant difference.

3. Results

3.1. Signal measurement and feature representation

Figure 4 shows typical recorded joint angles, intraspinal LFP activity, the amplitude of the LFP signal, the average of the power spectrum in the three logarithmically spaced frequency bands (0.5-30 Hz, 30-120 Hz, and 120-300 Hz), and corresponding time-frequency analysis during a

Accepted Manuscript

typical trial of active (cat 2, 73 days post-implant) and passive movement (cat 2, 29 days post-implant) of the hindlimb. It is seen that the LFP signal recorded from the dorsal column closely tracks the joint angle during both passive and active movement. During this trial of passive movement, almost a full-wave rectified sine wave pattern was generated for the three joints. Interestingly, the same wave pattern was produced by the neural activity in the spinal cord. Even, the effects of the small variations that occurred in cycles 2 and 3 of the ankle joint angle have appeared in the LFP signal. The frequency components could clearly reflect all changes in the joint angle patterns. Although the movement patterns (i.e., joint angle trajectories) generated during walking on the treadmill (figure 4(b)) were not regular as much as that during passive movement, the recorded spinal dorsal column neuronal responses could closely reflect the changes of the joint angles.

3.2. Regression contribution analysis

In this section, the results of the regression analysis are presented to investigate the contribution of the features, recording channels, and signal samples in decoding the hindlimb kinematics. Figure 5 shows the results of the regression analysis for five cats during walking on the treadmill. It can be seen that recording electrodes in both the LC and DC contributed to the decoding during active movement (figure 5(a)). However, the most lateral and the most dorsal electrodes show more contribution to the decoding performance in cats 1, 3, 4, and 5.

The contribution of the extracted features is shown in figure 5(b). The results of the two-way ANOVA show that there is a significant difference in the contribution of the features to the decoding process for all cats ($p < 0.0001$). The results of Tukey's HSD posthoc analysis show that, compared to the frequency bands, the amplitude of the LFP signal has a significant contribution to the movement decoding ($p < 0.01$). Moreover, the results show a statistically significant interaction between joint angles and features ($p < 0.03$). It can be seen that the contributions of the LF and HF bands are more than that of the MF bands for all cats and all joints. However, for some cats and some joints, this contribution is significant. For example, for the ankle joints of cats 2 and 3, the contributions of the LF and HF bands are significantly more than that of the MF band ($p < 0.01$).

Accepted Manuscript

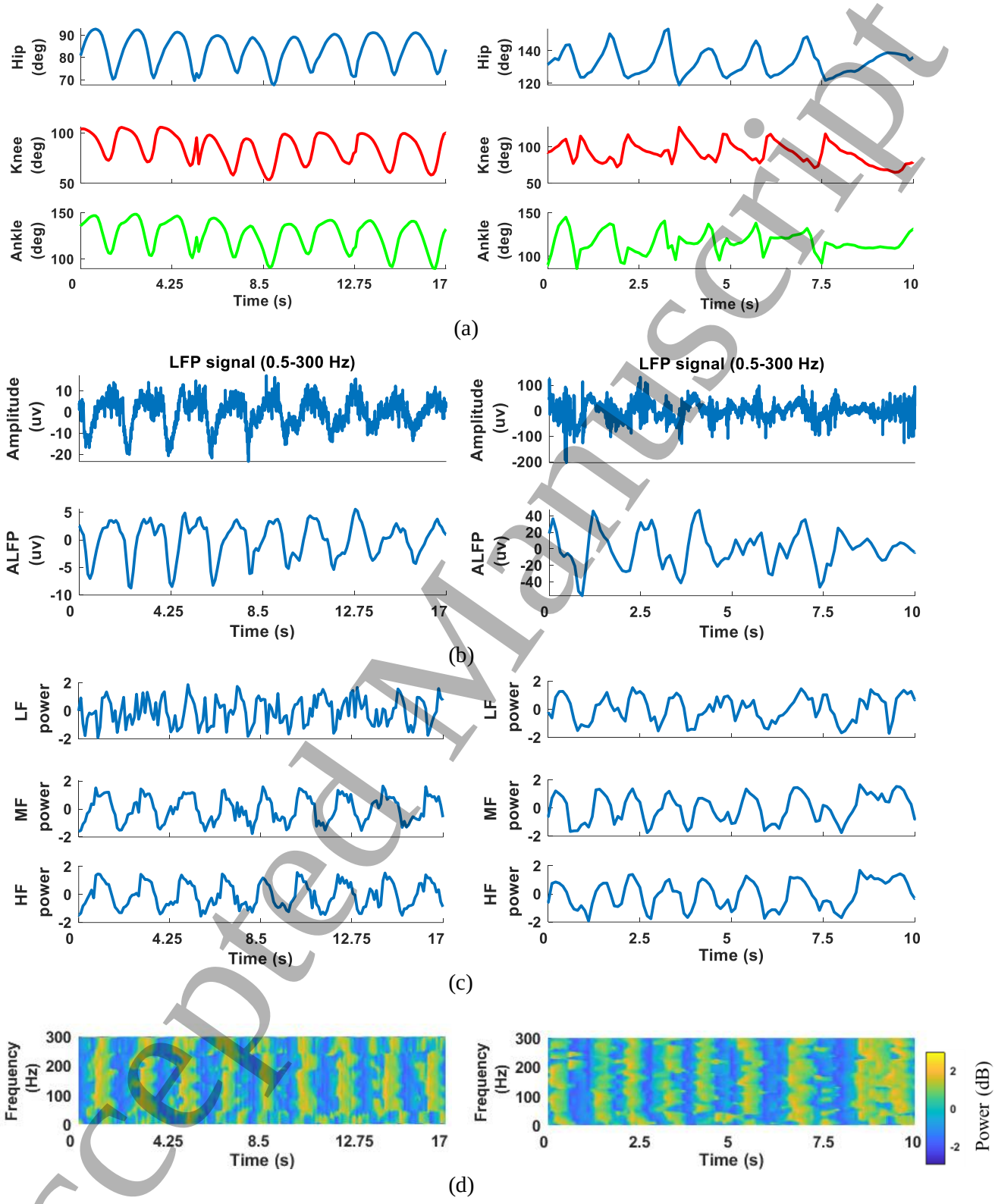

Figure 4. An example of the measured joint angles and neural signal recorded from the dorsal column during passive (left, cat 2, 29 days post-implant) and active (right, cat 2, 73 days post-implant) movements. (a) Measured joint angles. (b) Band-pass filtered (0.5-300 Hz) neural signal and corresponding amplitude of the LFP. (c) Frequency bands of the recorded neural signal. (d) Time-frequency representation of the LFP signal.

Accepted Manuscript

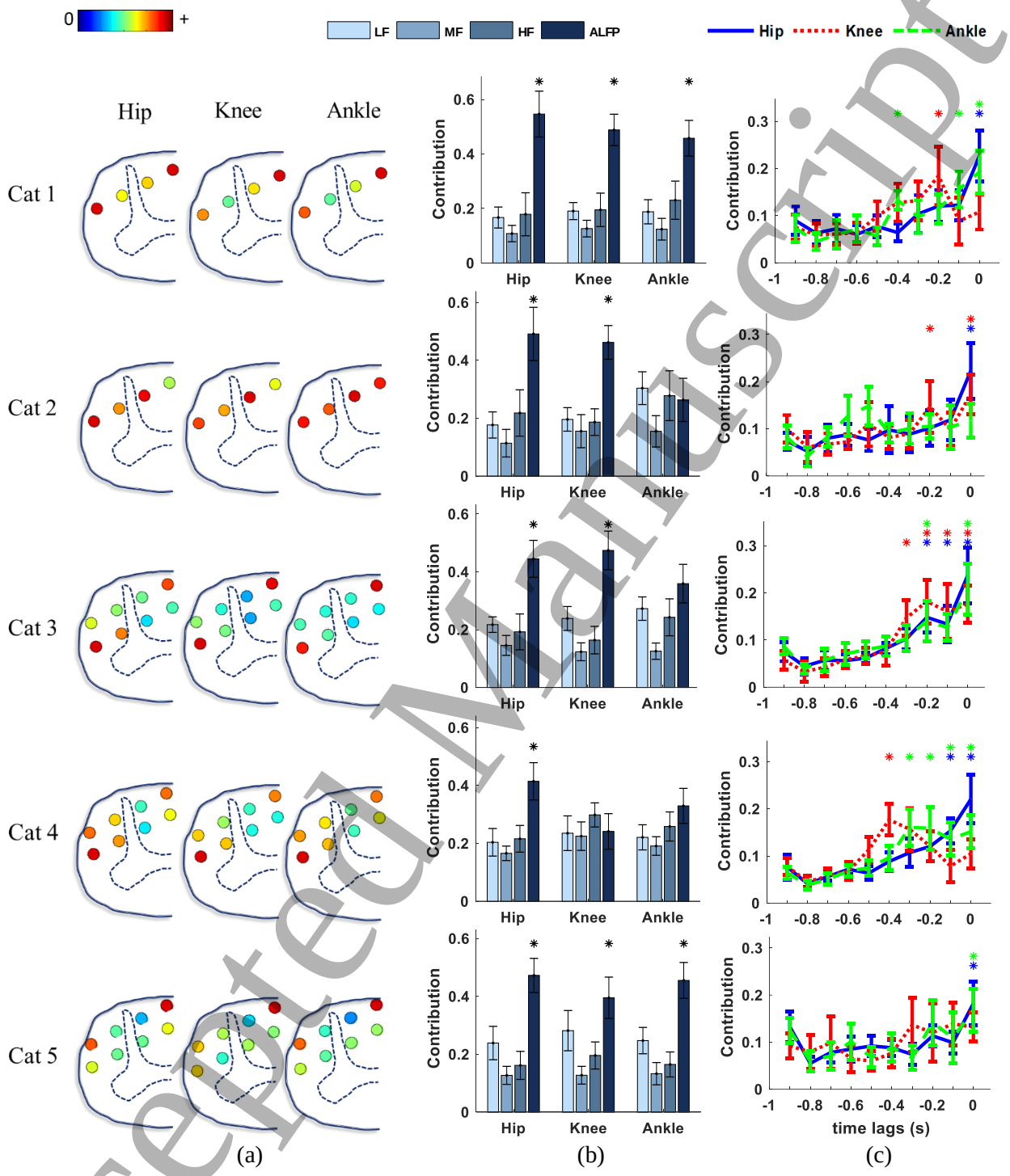

Figure 5. Regression contribution analysis using the coefficients of the decoding model across different joint angles and animals during cat walking freely on a treadmill. (a) Contributions of different recording channels, to the decoding hip, knee, and ankle angles (red color indicates the highest contribution and blue lowest contribution). (b) Contributions of features, to the decoding. Features with significantly greater contribution than others (based on one-way ANOVA for each angle) are shown by asterisks. (c) Temporal contributions of different time lags. Time lags with significantly greater contributions than their median are shown by asterisks. The error bar on each graph represents the standard deviation.

Accepted Manuscript

Significantly greater temporal contributions than their median ($p < 0.01$ one-way ANOVA followed by Tukey's HSD, asterisks in figure 5(c)) were found within 400 ms before the predicted instant. Here, the fifth lag was considered as the median. Temporal contribution decreases as the time lag increases.

Figure 6 shows the results of the regression analysis for five cats during the passive hindlimb movements of the anesthetized cats. The most contribution of the recording channels is related to the channels in the dorsal column. However, some contributions can be seen for recording channels in the lateral column for cats 1, 3, and 4.

Similar to regression analysis during walking on the treadmill, the amplitude of the LFP signal has also made a significant contribution to the movement decoding ($p < 0.0001$, two-way ANOVA followed by Tukey's HSD posthoc) during passive movements. Furthermore, the results show that there is no statistically significant interaction between joint angles and features ($p > 0.99$) during passive movement. The zero time lag in the input time series provides significantly greater temporal contributions than their median ($p < 0.01$ one-way ANOVA followed by Tukey's HSD). It is observed that the input with time lag 800 ms has the least contribution, but the contribution begins to increase for the time lag 900 ms for all cats. This may be due to the periodic nature of the movement pattern during passive experiments.

3.3. Mutual information analysis

In this section, the relative kinematic information of the extracted features and the recording channels in both the DC and the LC regions is investigated using MI analysis during active locomotion in awake cats and passive movement in anesthetized cats. For this purpose, the average of MI between each joint angle and each LFP features (LF, MF, HF, and ALFP) for each recording channel was computed. Then, the average of MI for each joint angle over the recording channels in the DC as well as LC regions was computed (figure 7).

A two-way ANOVA, considering electrode location (DC or LC) as the column factors and the features (LF, MF, HF, or AE) as the row factors, was performed and followed by Tukey's posthoc. The results show that the LFP amplitudes contain significantly more information than the frequency components ($p < 0.0001$) during both active locomotion and passive movement. It is interesting to note that there is no statistically significant difference between the information content of the signals recorded in the DC and LC regions ($p > 0.29$ and type II error of $\beta = 0.38$ at the significance level of $p = 0.05$) during active movement. But, the information content of the DC is significantly higher than that of the LC ($p < 0.01$) during passive movement.

Accepted Manuscript

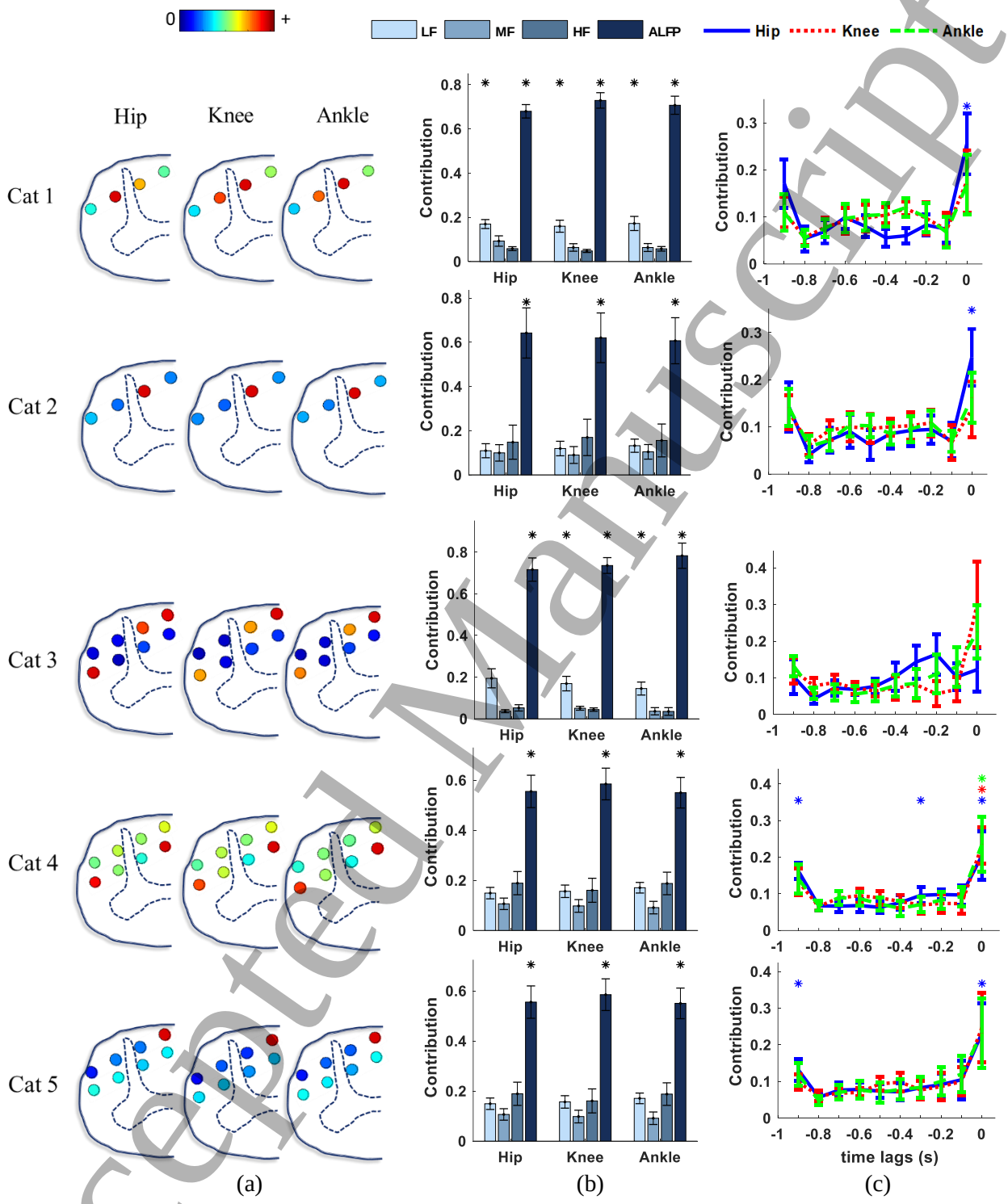

Figure 6. Regression contribution analysis using the coefficients of the decoding model across different joint angles and animals during passive movements. (a) Contributions of different recording channels, to the decoding hip, knee, and ankle angles (red color indicates the highest contribution and blue lowest contribution). (b) Contributions of features, to the decoding. Features with significantly greater contribution than others (based on one-way ANOVA for each angle) are shown by asterisks. (c) Temporal contributions of different time lags. Time lags with significantly greater contributions than their median are shown by asterisks. The error bar on each graph represents the standard deviation.

Accepted Manuscript

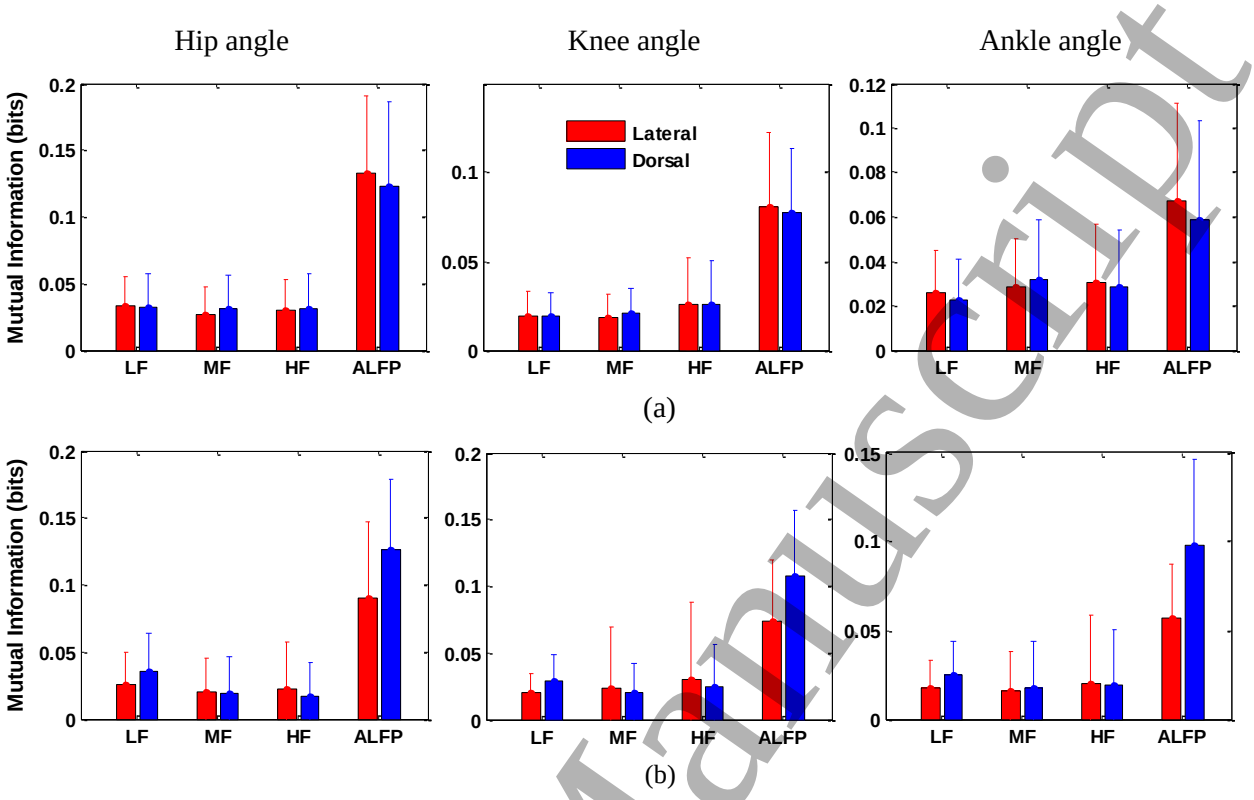

Figure 7. Mutual information between each feature (i.e., low frequency, mid-frequency, and high-frequency bands and averaged amplitude of LFP signal) that is extracted from the neural signals recorded from the lateral column (red) as well as the dorsal column (blue), and each joint angle trajectory during the active movement (a) and passive movement (b). The error bar on each bar graph represents the standard deviation.

We further calculated the MI values between LFP signals of different recording channels during active and passive movements, and the results are presented in figure 8. The results show that as the electrode inter-distance increases, the MI decreases. The average of the MI between the recording channels in the LC region, in the DC region, and between the recording channels in the DC and LC during both walking on the treadmill and passive movements is computed and is shown in figure 8(d). The results show that the MI between the recording channels in the DC and LC during walking on the treadmill is higher than that during passive movements ($p = 0.06$). Moreover, the MI between recording channels in the LC during walking on the treadmill is higher than that of passive movement ($p = 0.007$).

Accepted Manuscript

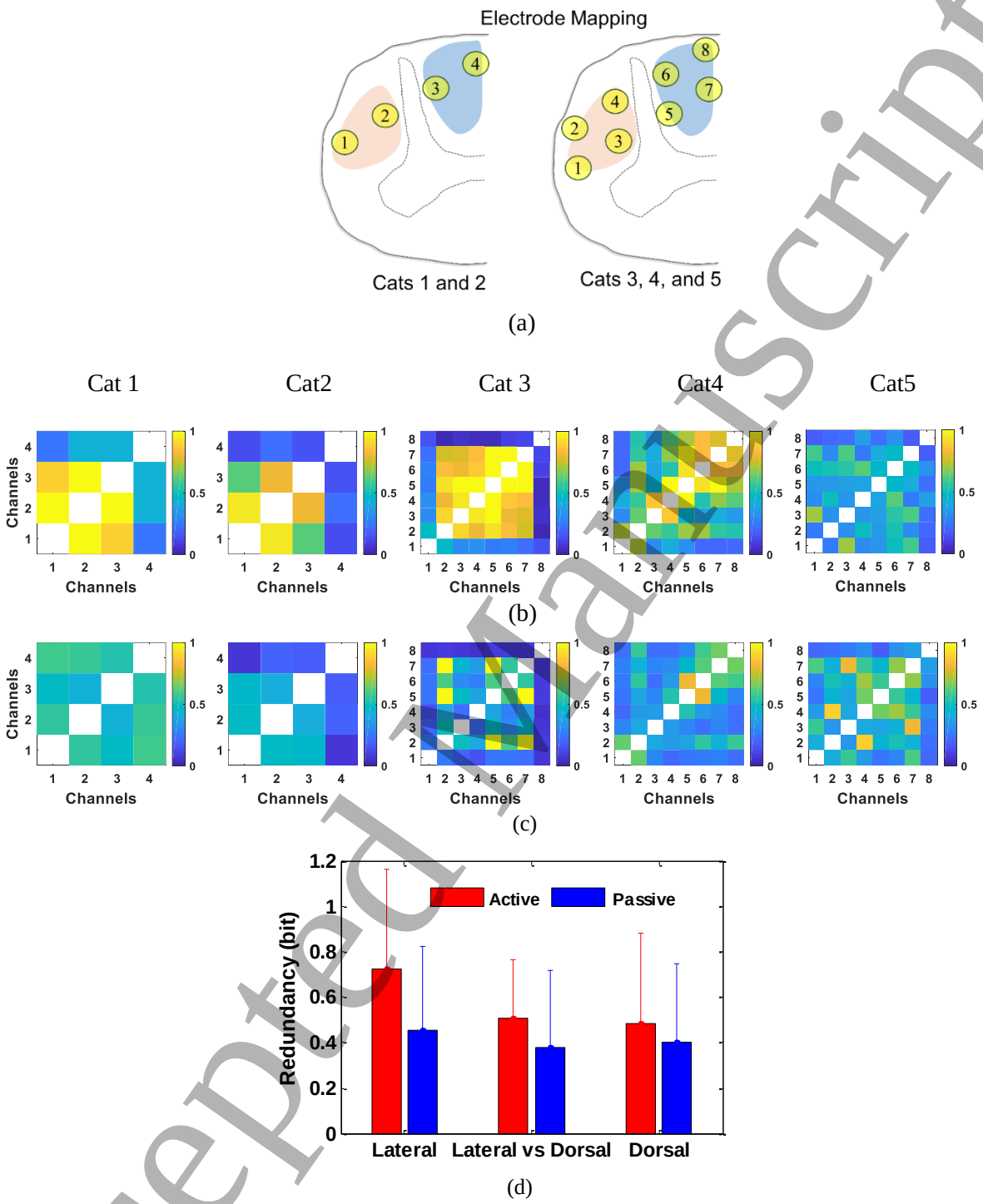

Figure 8. Mutual information between the LFP signals of different recording channels. (a) Schematic illustration of the spatial position of the implanted electrodes in the lateral and dorsal columns. (b) Mutual information between the recording channels during the active experiment. (c) Mutual information between the recording channels during the passive experiment. (d) Average of MI between recording channels in the LC region as well as the DC region and between the LC and DC regions. The error bar on each bar graph represents the standard deviation.

3.4 Decoding performance

Accepted Manuscript

Figure 9 shows an example of decoding the limb kinematics using the neural signals recorded from the recording channels in the DC region, in the LC region, or both in the DC and LC regions during active and passive experiments.

Figure 10 shows the average of the decoding performance using the recording channels in each region as well as in both regions. During walking on the treadmill, the averages of the coefficient of determination (R^2) are 0.33, 0.34, and 0.40 using the recording channels in the DC, the LC, and both in the DC and LC regions, respectively, and during passive movement are 0.53, 0.42, and 0.57. During walking on the treadmill, the average NRMS errors obtained are 0.15, 0.15, and 0.14 using the recording channels in the DC, in the LC, and both in the DC and LC regions, respectively, and during passive movement are 0.17, 0.19, and 0.16.

The results of statistical analysis show that there is no statistically significant difference between the decoding performance obtained by the recording channels in the DC and that obtained by the LC during walking on the treadmill ($p > 0.64$ and type II error $\beta = 0.27$ at the significance level of $p = 0.05$). But, during the passive movement, the decoding performance obtained using the recording channels in the DC is significantly different from that obtained using the channels in the LC ($p < 0.0001$).

The decoding performance obtained using all the recording channels both in the LC and DC regions is significantly better than that obtained using only the channels in the LC region ($p < 0.001$) during both active and passive experiments and significantly better than that obtained using the channels in the DC during awake experiments ($p < 0.001$). However, there is no significant difference between all channels and the DC during passive experiments.

3.5. Long-term stability of decoding performance

To evaluate the long-term signal quality, we calculated the decoding performance for each session of the experiment over a long-term period (about 2~3 months) (figure 11). The results of the statistical analysis based on the Spearman correlation test shows that there is no significant monotonic increase in NRMS values over time ($p > 0.1$ and $|\rho| < 0.4$). Also, the Spearman correlation test shows no monotonic decrease in R^2 values over time ($p > 0.01$ and $|\rho| < 0.64$).

Accepted Manuscript

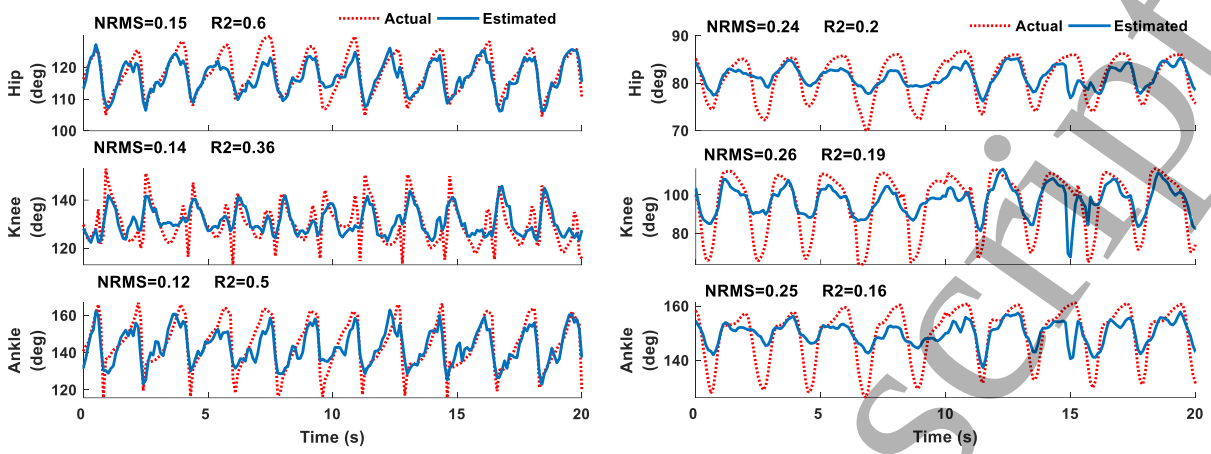

(a)

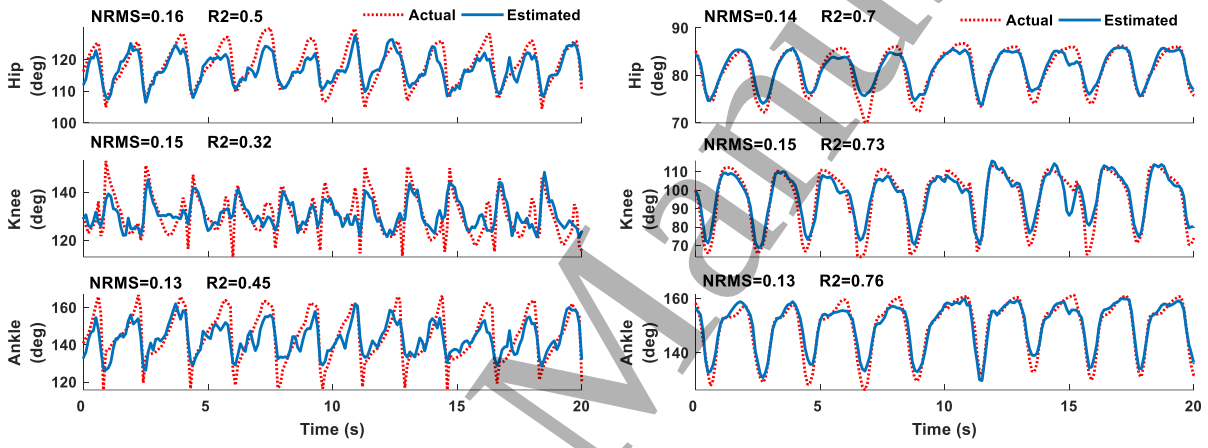

(b)

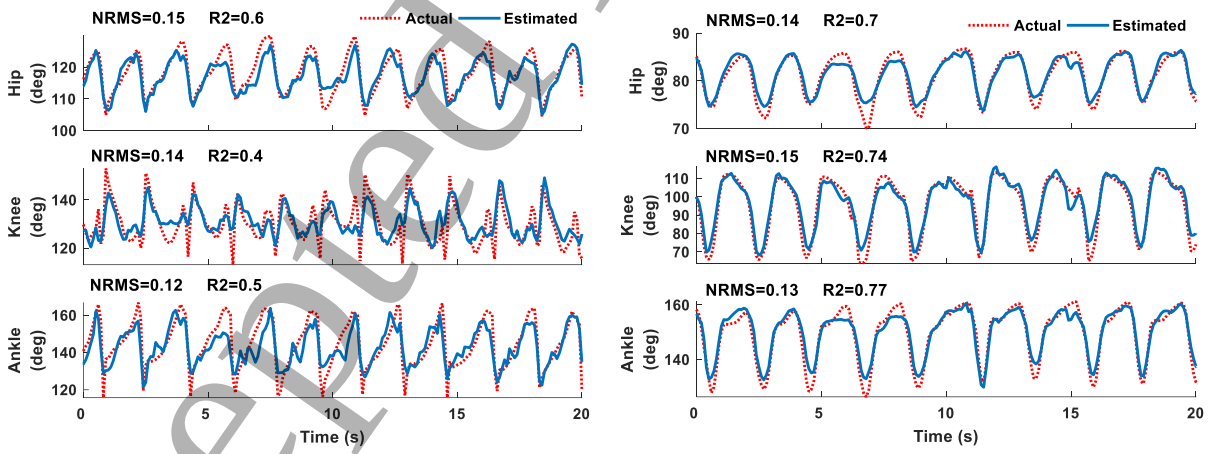

(c)

Figure 9. Examples of decoding the joint angles during active (left) and passive (right) movements. (a) Decoding using signals recorded from the lateral column. (b) Decoding using signals recorded from the dorsal column. (c) Decoding using signals recorded from both the dorsal and lateral columns. The results were obtained from cat 5, 42 days post-implant for active movement and 31 days post-implant for passive movement.

Accepted Manuscript

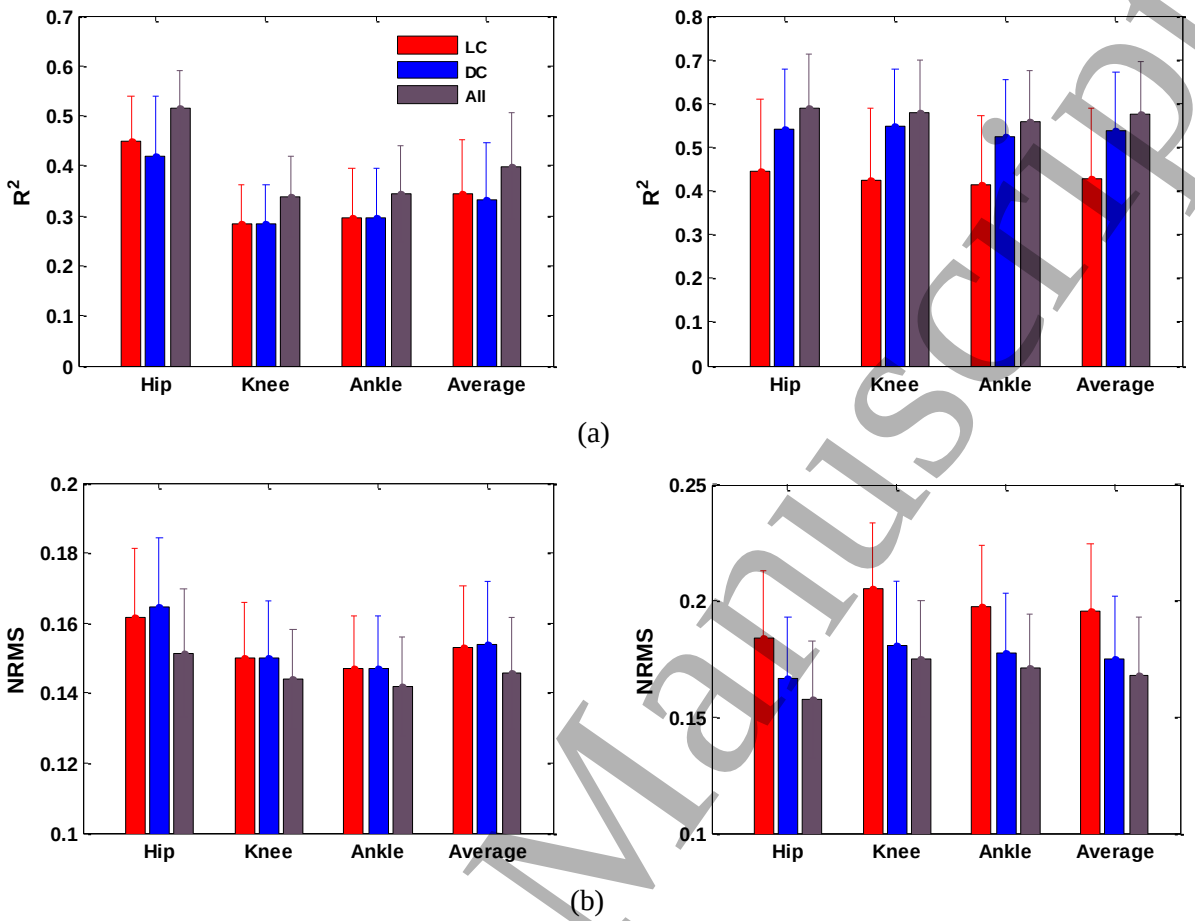

Figure 10. Average decoding performance during active (left) and passive (right) movements using the LFP signals recorded from electrodes implanted in the LC (red), in the DC (blue), and all electrodes implanted in both the LC and the DC reigns (brown). (a) Averaged R^2 values. (b) Averaged NRMS errors. The error bar on each bar graph represents the standard deviation.

4. Discussion and conclusions

This study addresses the problem of estimating the hindlimb kinematics using neural signals recorded from the spinal cord. In contrast to our previous work, which provided decoding the hindlimb kinematics from multi-segment recordings of the dorsal horn neurons during passive movement, the current study addresses the problem of estimating the hindlimb information the ascending and descending tracts during walking on the treadmill as well as passive movement. A custom microwire array was designed such that both dorsal and lateral columns in the spinal cord were mediolaterally and dorsoventrally covered.

Accepted Manuscript

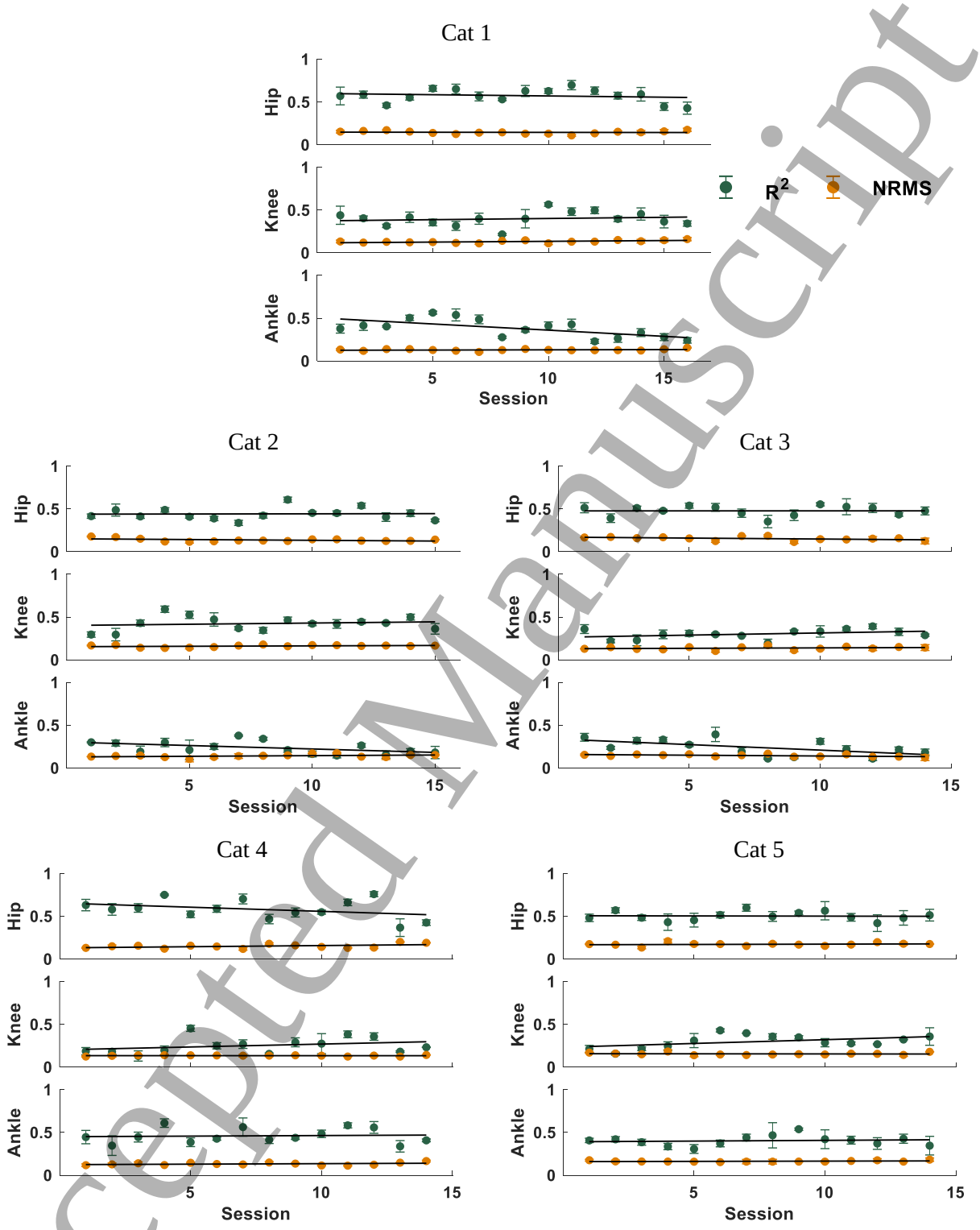

Figure 11. Long-term decoding performance during walking on the treadmill. R^2 and NRMS values for each joint angle and each animal show no significant decrease over the recording period.

The results of the regression contribution analysis indicated that the recording electrodes in both the LC and DC contributed to the decoding during active movement. However, the most

Accepted Manuscript

lateral and the most dorsal electrodes show more contribution to the decoding performance. In contrast, the most contribution of the recording channels is related to the channels in the dorsal column during the passive movement. The results of mutual information analysis and decoding performance confirm this contribution. There is no statistically significant difference between the information content of the signals recorded in the DC and LC regions ($p > 0.29$) during active movement, but the information content of the DC is significantly higher than that of the LC ($p < 0.01$) during passive movement. The results also show that there is no statistically significant difference ($p > 0.64$) between the decoding performances obtained by the channels in the LC region and DC region during walking on the treadmill. But, during the passive movement, the decoding performance obtained using the recording channels in the DC is significantly better than that obtained using the channels in the LC ($p < 0.0001$). The results of this analysis indicate that the descending tracts in the spinal cord can be considered as a source for extracting the motor commands and the ascending neural signals in the spinal cord as the feedback information for neuroprosthetic applications.

The regression analysis results about the contribution of the frequency bands show that the LF and HF bands convey more information about the limb movement than the MF band. Interestingly, these findings are almost in agreement with the previously published literature about the role of frequency components of the LFP signal recorded from the brain [57-62]. It has been shown that the theta rhythm (e.g., 6-12 Hz) in the subcortical regions is associated with the movement dynamics (e.g., speed of locomotion and transition from resting to locomotion) [57-59]. The neural oscillations in the entire gamma range (30-120 Hz) are associated with decision-making, increased attention, and improved reaction times [60]. Higher-frequency band (>100 Hz) provides indirect access to the spike outputs of neurons [61]. In our previous work [62], it was shown that the high-frequency band of ECoG signal inside the range of 200-400 Hz contain significant information about the movement dynamics.

A problem facing the cortically driven brain-computer interface for control of locomotion is the lack of signals derived from subcortical centers involving in initiation, regulation, and decision making, such as the midbrain, hindbrain, cerebellum, brain stem, and basal ganglia [40, 53-56]. A potential solution for this problem would be to extract the details of motor execution using the descending signals in the spinal cord, while the cortically driven brain-computer interface can be utilized for extracting the high-level motor command information. The results of this analysis show

Accepted Manuscript

that the low-level execution of the motor execution can be extracted from descending signals in the spinal cord.

The results of this study show that the recorded spinal signals could closely track the joint angle trajectories using a linear model. The decoding performance can be improved by using nonlinear methods and will be considered as the object of the future study. The validation of the current study was limited to within-session cross-fold-validation. From a practical standpoint, it is compelling to train a model for a subject and could transfer the learning to different subjects and different sessions. Non-stationarity and low signal-to-noise ratio (SNR) characteristics of the neural signals, electrode displacement, and electrode-tissue impedance variations are grand challenges to design a universal machine leaning model that is optimal for different subjects and different sessions of experiment. To cope with this problem, various machine learning algorithms such as active learning and transfer learning (TL) have been proposed by the researchers. In TL, the data from relevant subjects or sessions were used to facilitate learning for a new subject or new session. Utilizing the TL for building a general decoding model could be explored in future studies.

Another critical issue in decoding the hindlimb kinematics as the feedback information for control of FES is the long-term stability. Unfortunately, there is a lack of reports on investigating the long-term stability of decoding using neural signals recorded from the spinal cord. The results of this work show that stable decoding performance can be achieved over 8 to 14 weeks without significant monotonic degradation of performance.

Fabrication and implantation of the intraspinal microwires are other challenges facing the neural recording from the spinal cord. Additionally, implanting microwires into the body always carries the risk of infection and migration. However, recent progress in microwire fabrication and knowledge gained from implantable electrodes on animals [63-65] can be applied to a chronically implanted prosthetic device.

As a concluding remark, this work presents a promising approach to developing neuroprosthetic systems that provide an interface between the above and below the level of spinal cord injury using the descending neural signal in the spinal cord.

Data availability

All datasets obtained during the current study are available from the corresponding author on reasonable request.

Accepted Manuscript

Acknowledgments

This work was supported by the Iran Neural Technology Research Center, Tehran, Iran, under Grant 48.M.111194. There are no conflicts of interest for the authors of this study.

References

[1] Collinger J L, Foldes S, Bruns T M, Wodlinger B, Gaunt R and Weber D J 2013 Neuroprosthetic technology for individuals with spinal cord injury *J. Spinal Cord Med.* **36** 258–72

[2] Fitzsimmons N A, Lebedev M A, Peikon I D and Nicolelis M A L 2009 Extracting kinematic parameters for monkey bipedal walking from cortical neuronal ensemble activity *Front. Integr. Neurosci.* **3** 1–19

[3] Rigosa J, Panarese A, Dominici N, Friedli L, van den Brand R, Carpaneto J, DiGiovanna J, Courtine G and Micera S 2015 Decoding bipedal locomotion from the rat sensorimotor cortex *J. Neural Eng.* **12** 056014

[4] Song W, Ramakrishnan A, Udoekwere U I and Giszter S F 2009 Multiple types of movement-related information encoded in hindlimb/trunk cortex in rats and potentially available for brain–machine interface controls *IEEE Trans. Biomed. Eng.* **56** 2712–6

[5] Barroso F O et al 2019 Decoding neural activity to predict rat locomotion using intracortical and epidural arrays *J. Neural Eng.* **16** 036005

[6] Riso R R, Mosallaie F K, Jensen W and Sinkjaer T 2000 Nerve cuff recordings of muscle afferent activity from tibial and peroneal nerves in rabbit during passive ankle motion *IEEE Trans. Rehabil. Eng.* **8** 244–58

[7] Micera S, Jensen W, Sepulveda F, Riso R R and Sinkjaer T 2001 Neuro-fuzzy extraction of angular information from muscle afferents for ankle control during standing in paraplegic subjects : an animal model *IEEE Trans. Biomed. Eng.* **48** 787–94

[8] Song K Il, Chu J U, Park S E, Hwang D and Youn I 2017 Ankle-angle estimation from blind source separated afferent activity in the sciatic nerve for closed-loop functional neuromuscular stimulation system *IEEE Trans. Biomed. Eng.* **64** 834–43

[9] Hansen M, Haugland M K and Sinkjær T 2004 Evaluating robustness of gait event detection based on machine learning and natural sensors *IEEE Trans. Neural Syst. Rehabil. Eng.* **12** 81–8

[10] Eggers T E, Dweiri Y M, Mccallum G A and Durand D M 2018 Recovering motor activation with chronic peripheral nerve computer interface *Sci. Rep.* **8** 14149

[11] Micera S et al 2011 Decoding of grasping information from neural signals recorded using peripheral intrafascicular interfaces *J. Neuroeng. Rehabil.* **8** 1–10

[12] Cracchiolo M, Valle G, Petrini F, Strauss I, Granata G, Stieglitz T, Rossini P M, Raspopovic S, Mazzoni A and Micera S M 2020 Decoding of grasping tasks from intraneural recordings in trans-radial amputee *J. Neural Eng.* **17** 026034

[13] Haugland M K and Sinkjær T 1995 Cutaneous whole nerve recordings used for correction of footdrop in hemiplegic man *IEEE Trans. Rehabil. Eng.* **3** 307–17

[14] Micera S and Raspopovic S 2010 Control of hand prostheses using peripheral information *IEEE*

Accepted Manuscript

Rev. Biomed. Eng. **3** 48–68

[15] Hong K, Aziz N and Ghafoor U 2018 Motor-commands decoding using peripheral nerve signals : a review *J. Neural Eng. Top.* **15** 031004

[16] Weber D J, Stein R B, Everaert D G and Prochazka A 2006 Decoding sensory feedback from firing rates of afferent ensembles recorded in cat dorsal root ganglia in normal locomotion *IEEE Trans. Neural Syst. Rehabil. Eng.* **14** 240–3

[17] Weber D J, Stein R B, Everaert D G and Prochazka A 2007 Limb-state feedback from ensembles of simultaneously recorded dorsal root ganglion neurons. *J. Neural Eng.* **4** S168–80

[18] Rigosa J, Weber D J, Prochazka A, Stein R B and Micera S 2011 Neuro-fuzzy decoding of sensory information from ensembles of simultaneously recorded dorsal root ganglion neurons for functional electrical stimulation applications. *J. Neural Eng.* **8** 046019

[19] Stein R B, Weber D J, Aoyagi Y, Prochazka A, Wagenaar J B M, Shoham S and Normann R A 2004 Coding of position by simultaneously recorded sensory neurones in the cat dorsal root ganglion *J. Physiol.* **560** 883–96

[20] Wagenaar J B, Ventura V and Weber D J 2011 State-space decoding of primary afferent neuron firing rates *J. Neural Eng.* **8** 016002

[21] Bruns T M, Wagenaar J B, Bauman M J, Gaunt R A and Weber D J 2013 Real-time control of hind limb functional electrical stimulation using feedback from dorsal root ganglia recordings *J. Neural Eng.* **10** 026020

[22] Holinski B J, Everaert D G, Mushahwar V K and Stein R B 2013 Real-time control of walking using recordings from dorsal root ganglia *J. Neural Eng.* **10** 056008

[23] Han S, Chu J-U, Kim H, Park J W and Youn I 2017 Multiunit activity-based real-time limb-state estimation from dorsal root ganglion recordings *Sci. Rep.* **7** 44197

[24] Kashkoush A I, Gaunt R A and Weber D J 2019 Recording single- and multi-unit neuronal action potentials from the surface of the dorsal root ganglion *Sci. Rep.* **9** 1–12

[25] Debnath S, Bauman M J, Fisher L E, Weber D J and Gaunt R A 2014 Microelectrode array recordings from the ventral roots in chronically implanted cats *Front. Neurol.* **5** 1–9

[26] Bauman M J 2019 A ventral root interface for neuroprosthetic control of locomotion *Doctoral Dissertation*, University of Pittsburgh.

[27] Bosco G and Poppele R E 2000 Reference frames for spinal proprioception: kinematics based or kinetics based? *J. Neurophysiol.* **83** 2946–55

[28] Bosco G and Poppele R E 2001 Proprioception from a spinocerebellar perspective. *Physiol. Rev.* **81** 539–68

[29] Bosco G 2003 Modulation of dorsal spinocerebellar responses to limb movement. II. effect of sensory input *J. Neurophysiol.* **90** 3372–83

[30] Bosco G, Eian J and Poppele R E 2006 Phase-specific sensory representations in spinocerebellar activity during stepping: evidence for a hybrid kinematic/kinetic framework *Exp. Brain Res.* **175** 83–96

[31] Kandel E R, Schwartz J H, Jessell T M, Siegelbaum S A and Hudspeth A J 2000 Principles of Neural Science (New York: McGraw-hill)

Accepted Manuscript

[32] Borisoff J F, Mcphail L T, Saunders J T W, Birch G E and Ramer M S 2006 Detection and classification of sensory information from acute spinal cord recordings *IEEE Trans. Biomed. Eng.* **53** 1715–19

[33] Im C, Park H Y, Koh C S, Ryu S B, Seo I S, Kim Y J, Kim K H and Shin H C 2016 Decoding intravesical pressure from local field potentials in rat lumbosacral spinal cord *J. Neural Eng.* **13** 056005

[34] Jabbari M and Erfanian A 2019 Estimation of bladder pressure and volume from the neural activity of lumbosacral dorsal horn using a long-short-term-memory-based deep neural network *Sci. Rep.* **9** 18128

[35] Yeganegi H, Fathi Y and Erfanian A 2018 Decoding hind limb kinematics from neuronal activity of the dorsal horn neurons using multiple level learning algorithm *Sci. Rep.* **8** 577

[36] Fathi Y and Erfanian A 2019 A probabilistic recurrent neural network for decoding hind limb kinematics from multi-segment recordings of the dorsal horn neurons *J. Neural Eng.* **16** 036023

[37] Lemon R N 2008 Descending pathways in motor control *Annu. Rev. Neurosci.* **31** 195–218

[38] Rossignol S, Barrière G, Alluin O and Frigon A 2009 Re-expression of locomotor function after partial spinal cord injury *Physiology* **24** 127–39

[39] Frigon A, Rossignol S and Frigon A 2011 Recovery of locomotion after spinal cord injury : some facts and mechanisms *Annu. Rev. Neurosci.* **34** 413–40

[40] Takakusaki K, Chiba R, Nozu T and Okumura T 2016 Brainstem control of locomotion and muscle tone with special reference to the role of the mesopontine tegmentum and medullary reticulospinal systems. *J. Neural Transm.* **123** 695–729.

[41] Prasad A and Sahin M 2006 Extraction of motor activity from the cervical spinal cord of behaving rats *J. Neural Eng.* **3** 287–92

[42] Prasad A and Sahin M 2010 Characterization of neural activity recorded from the descending tracts of the rat spinal cord *Front. Neurosci.* **4** 1–7

[43] Prasad A and Sahin M 2012 Can motor volition be extracted from the spinal cord? *J. Neuroeng. Rehabil.* **9** 41

[44] Guo Y, Foulds R A, Adamovich S V. and Sahin M 2014 Encoding of forelimb forces by corticospinal tract activity in the rat *Front. Neurosci.* **8** 62

[45] Guo Y, Gok S and Sahin M 2018 Convolutional networks outperform linear decoders in predicting EMG from spinal cord signals *Front. Neurosci.* **12** 689

[46] Gok S and Sahin M 2019 Prediction of forelimb EMGs and movement phases from corticospinal signals in the rat during the reach-to-pull task *Int. J. Neural Syst.* **29** 1950009

[47] Zou H and Hastie T 2005 Regularization and variable selection via the elastic net *Journal of the royal statistical society: series B (statistical methodology)* **67** 301–20

[48] Friedman J, Hastie T and Tibshirani R 2010 Regularization paths for generalized linear models via coordinate descent *J. Stat. Softw.* **33** 1–22

[49] Efron B, Hastie T, Johnstone I and Tibshirani R 2004 Least angle regression *Ann. Stat.* **32** 407–99

[50] Darbellay G A and Vajda I 1999 Estimation of the information by an adaptive partitioning of the observation space *IEEE Trans. Inf. Theory* **45** 1315–21

Accepted Manuscript

[51] Chao Z C, Nagasaka Y and Fujii N 2010 Long-term asynchronous decoding of arm motion using electrocorticographic signals in monkeys *Front. Neuroeng.* **3** 3

[52] Choi H, Lee J, Park J, Lee S, Ahn K, Kim I Y, Lee K-M and Jang D P 2018 Improved prediction of bimanual movements by a two-staged (effector-then-trajectory) decoder with epidural {ECoG} in nonhuman primates *J. Neural Eng.* **15** 16011

[53] Drew T, Andujar J-E, Lajoie K and Yakovenko S 2008 Cortical mechanisms involved in visuomotor coordination during precision walking *Brain Res. Rev.* **57** 199–211

[54] Drew T and Marigold D S 2015 Taking the next step: cortical contributions to the control of locomotion *Curr. Opin. Neurobiol.* **33** 25–33

[55] Takakusaki K 2008 Forebrain control of locomotor behaviors *Brain Res. Rev.* **57** 192–198.

[56] Grillner S and Robertson B 2015 The basal ganglia downstream control of brainstem motor centres – an evolutionarily conserved strategy. *Curr. Opin. Neurobiol.* **33** 47–52

[57] Ledberg A and Robbe D 2011 Locomotion-related oscillatory body movements at 6-12 Hz modulate the hippocampal theta rhythm *PLoS One* **6** e27575

[58] Bender F, Gorbati M, Cadavieco M C, Denisova N, Gao X, Holman C, Korotkova T and Ponomarenko A 2015 Theta oscillations regulate the speed of locomotion via a hippocampus to lateral septum pathway *Nat. Commun.* **6** 8521

[59] Noga B R, Sanchez F J, Villamil L M, O'Toole C, Kasicki S, Olszewski M, Cabaj A M, Majczyński H, Sławińska U and Jordan L M 2017 LFP oscillations in the mesencephalic locomotor region during voluntary locomotion *Front. Neural Circuits* **11** 34

[60] Ahmed O J and Mehta M R 2012 Running speed alters the frequency of hippocampal gamma oscillations *J. Neurosci.* **32** 7373–83

[61] Buzsáki G, Anastassiou C A and Koch C 2012 The origin of extracellular fields and currents — EEG, ECoG, LFP and spikes *Nat. Rev. Neurosci.* **13** 407–20

[62] Farrokhi B and Erfanian A 2018 A piecewise probabilistic regression model to decode hand movement trajectories from epidural and subdural ECoG signals *J. Neural Eng.* **15** 036020

[63] Bamford J A, Lebel R M, Parseyan K and Mushahwar V K 2016 The fabrication , implantation and stability of intraspinal microwire arrays in the spinal cord of cat and rat *IEEE Trans. Neural Syst. Rehabil. Eng.* **25** 287–96

[64] Toossi A, Everaert D G, Azar A, Dennison C R and Mushahwar V K 2017 Mechanically stable intraspinal microstimulation implants for human translation *Annu. Biomed. Eng.* **45** 681–94

[65] Toossi A, Everaert D G, Seres P, Jaremko J L, Robinson K, Kao C C, Konrad P E and Mushahwar V K 2018 Ultrasound-guided spinal stereotactic system for intraspinal implants *J. Neurosurg. Spine* **29** 292–305

Accepted Manuscript